Ablation of Grb10 Specifically in Muscle Impacts Muscle Size and Glucose Metabolism in Mice

Lowenna J. Holt,[1]* Amanda E. Brandon,[1,2]* Lewin Small,[1] Eurwin Suryana,[1] Elaine Preston,[1] Donna Wilks,[1] Nancy Mokbel,[1] Chantal A. Coles,[3] Jason D. White,[3,4] Nigel Turner,[1,5] Roger J. Daly,[6,7†] and Gregory J. Cooney[1,2†]

[1]Diabetes and Metabolism Division, Garvan Institute of Medical Research, Sydney, New South Wales 2010, Australia; [2]School of Medical Sciences, Charles Perkins Centre, University of Sydney, Sydney, New South Wales 2006, Australia; [3]Murdoch Children's Research Institute, Royal Children's Hospital, Parkville, Victoria 3052, Australia; [4]Department of Veterinary Biosciences, Faculty of Veterinary and Agricultural Science, University of Melbourne, Parkville, Victoria 3010, Australia; [5]Department of Pharmacology, University of New South Wales, Sydney, New South Wales 2052, Australia; [6]Cancer Program, Biomedicine Discovery Institute, Monash University, Clayton, Victoria 3800, Australia; and [7]Department of Biochemistry and Molecular Biology, Monash University, Clayton, Victoria 3800, Australia

Grb10 is an adaptor-type signaling protein most highly expressed in tissues involved in insulin action and glucose metabolism, such as muscle, pancreas, and adipose. Germline deletion of Grb10 in mice creates a phenotype with larger muscles and improved glucose homeostasis. However, it has not been determined whether Grb10 ablation specifically in muscle is sufficient to induce hypermuscularity or affect whole body glucose metabolism. In this study we generated muscle-specific Grb10-deficient mice (Grb10-mKO) by crossing $Grb10^{flox/flox}$ mice with mice expressing Cre recombinase under control of the human α-skeletal actin promoter. One-year-old Grb10-mKO mice had enlarged muscles, with greater cross-sectional area of fibers compared with wild-type (WT) mice. This degree of hypermuscularity did not affect whole body glucose homeostasis under basal conditions. However, hyperinsulinemic/euglycemic clamp studies revealed that Grb10-mKO mice had greater glucose uptake into muscles compared with WT mice. Insulin signaling was increased at the level of phospho-Akt in muscle of Grb10-mKO mice compared with WT mice, consistent with a role of Grb10 as a modulator of proximal insulin receptor signaling. We conclude that ablation of Grb10 in muscle is sufficient to affect muscle size and metabolism, supporting an important role for this protein in growth and metabolic pathways. (*Endocrinology* 159: 1339–1351, 2018)

Grb10 belongs to a family of highly related multi-domain adaptors that bind particular activated receptor tyrosine kinases and tyrosine-phosphorylated signaling proteins and regulate downstream signaling (1). Unique to this family is the BPS region, located between the PH and SH2 domains, which mediates binding to the insulin receptor (IR) and functions as a pseudosubstrate inhibitor (2). The SH2 domain is the primary binding module for other receptors, such as the insulinlike growth factor receptor (IGFR), growth hormone receptor, fibroblast growth factor receptor, and hepatocyte growth factor receptor (or cMet). Notably, these are all involved in muscle development and growth. Grb10 is most highly expressed in several tissues that are involved in insulin action and glucose metabolism, such as muscle, adipose, and pancreas (3, 4). It is also highly expressed in the brain.

ISSN Online 1945-7170

Received 19 September 2017. Accepted 17 January 2018.
First Published Online 23 January 2018

*Joint first authors.
†Joint senior authors.

Abbreviations: ANOVA, analysis of variance; cDNA, complementary DNA; EDL, extensor digitorum longus; Grb10-mKO, muscle-specific Grb10-deficient mice; HSA, human α-skeletal actin; IGF-1, insulinlike growth factor 1; IGFR, insulinlike growth factor receptor; IR, insulin receptor; IRS, insulin receptor substrate; KO, knockout; mRNA, messenger RNA; NEFA, nonesterified fatty acid; NHMRC, National Health and Medical Research Council of Australia; PCR, polymerase chain reaction; R_d, rate of disappearance; SEM, standard error of the mean; TA, tibialis anterior; WT, wild-type.

Grb10 is an imprinted gene that is important in development. In the mouse, Grb10 is expressed mostly from the maternal allele, but in the brain of mice it is paternally expressed. Global disruption of the maternal copy leads to overgrowth of the embryo and placenta in mice (3, 5, 6). Adult Grb10 knockout (KO) mice also have an increased body weight, accounted for by an increase in lean mass (3, 4, 7). Studies from our laboratory and others have shown that in these mice loss of Grb10 results in increased signaling through the IR in both muscle and white adipose tissue, increased glucose uptake, and increased whole body glucose homeostasis (3, 4, 7). More recently, we have identified a role for Grb10 in regulating muscle mass whereby Grb10 KO mice display hyperplasia, with no concurrent increase in myofiber size (6). This model of hypermuscularity is unlike other models such as insulinlike growth factor 1 (IGF-1) transgenic mice (8, 9) and myostatin KO mice (10), which exhibit both hyperplasia and hypertrophy. Our findings highlighted an important role for Grb10 in normal regulation of embryonic muscle development.

Although it is now well established that global deletion of Grb10 in mice increases muscle mass, increases muscle insulin action, and improves metabolic health, the relative contribution of different tissues to this phenotype remains to be clarified. Individual tissues have their own unique role to play in contributing to the overall phenotype of a global KO mouse. For example, pancreas-specific deletion of Grb10 leads to increased total pancreas weight with increased β-cell mass and insulin content. In addition, in Grb10-pancreas KO mice, insulin and IGF-1 signaling is increased in islets, insulin secretion is elevated, and whole body glucose tolerance is improved (11). In the case of adipose-specific deletion of Grb10, the resulting phenotype is one of enlarged fat pads (12). This effect is unlike that of the global KO mice, which have reduced fat depots. This study in particular highlights the autonomous role of Grb10 in adipose tissue, which is masked in the global KO. Clearly there are multiple and complex tissue interactions that contribute to overall body composition and metabolic profile. The autonomous role of Grb10 in muscle has not previously been examined.

Here, we report deletion of Grb10 specifically in muscle by using Cre recombinase under the control of the human α-skeletal actin (HSA) promoter to examine the impact on muscle mass and whole body glucose metabolism. We found no difference in muscle mass between wild-type (WT) and muscle-specific Grb10-deficient (Grb10-mKO) mice during early adulthood, but at 1 year of age the muscles were enlarged by fiber hypertrophy. At this age, the increase in muscle mass did not affect whole body glucose homeostasis under basal conditions. However, under the hyperinsulinemic conditions of a hyperinsulinemic/euglycemic clamp, Grb10-mKO mice had greater glucose uptake into muscle compared with WT mice. In addition, insulin signaling was increased, as evidenced by increased phospho-Akt levels. The results of this study support an autonomous role for Grb10 in muscle, highlighting the important regulatory role that this protein plays in both muscle size and muscle metabolism.

Materials and Methods

Animal maintenance and generation of Grb10-mKO mice

All animal studies were undertaken with the approval of the Garvan Institute/St Vincent's Hospital Animal Ethics Committee, according to guidelines issued by the National Health and Medical Research Council of Australia (NHMRC). Animals had *ad libitum* access to water and standard chow diet and were kept on a 12-hour light-dark cycle. To generate $Grb10^{flox/flox}$ (C57BL/6) mice, we targeted the *Grb10* allele by inserting loxP sites as shown in Fig. 1A. Cre recombinase action excises exon 4 and subsequently disrupts expression of the Grb10 protein. Female $Grb10^{flox/flox}$ mice were crossed with male mice expressing Cre recombinase from the HSA promoter (13). This strategy generates compound heterozygote mice that exhibit a deletion of Grb10 protein in muscle because the WT paternal allele is silent, whereas the floxed maternal allele gets disrupted by the action of the Cre. Floxed littermates were used as controls.

Hyperinsulinemic-euglycemic clamp studies

At 1 year of age, a cohort of mice were anesthetized with isoflurane anesthesia (4% induction, 1.5% to 2% maintenance) for insertion of catheters into the left carotid artery and right jugular vein (14). Free catheter ends were tunneled under the skin, externalized at the neck, and sealed. Mice were then singly housed and monitored daily. Catheters were flushed every 1 to 2 days with heparinized saline to maintain patency. Approximately 4 to 7 days after surgery, and after a ~5-hour fast, a hyperinsulinemic-euglycemic clamp was conducted. Mice were conscious and unrestrained and were not handled during the procedure to minimize stress. At −90 minutes, a primed (5 μCi) continuous infusion (0.05 μCi/min) of [3,^{3}H]-glucose (PerkinElmer) was commenced. At −30, −20, −10, and 0 minutes, samples were collected for basal rate of glucose disappearance (R_d) and glucose and insulin levels (−30 and 0). At time 0, the rate of [3,^{3}H]-glucose was increased (0.1 μCi/min), and a primed (16 mU/Kg), continuous (5 mU/kg/min) infusion of insulin commenced (Actrapid; Novo Nordisk, Copenhagen, Denmark). Glucose (25%) was infused at a variable rate to maintain glycemia at ~8 mM. Once blood glucose was stable, four sequential samples were taken for insulin and glucose turnover. A bolus of 2[^{14}C]deoxyglucose (13 μCi; PerkinElmer) was then administered and blood sampled at 2, 5, 10, 15, 20, and 30 minutes for measurement of glucose uptake into specific tissues. Animals were then euthanized and organs removed, snap frozen in liquid nitrogen, and stored at −80°C for additional analysis. This protocol is based on (15) and (16).

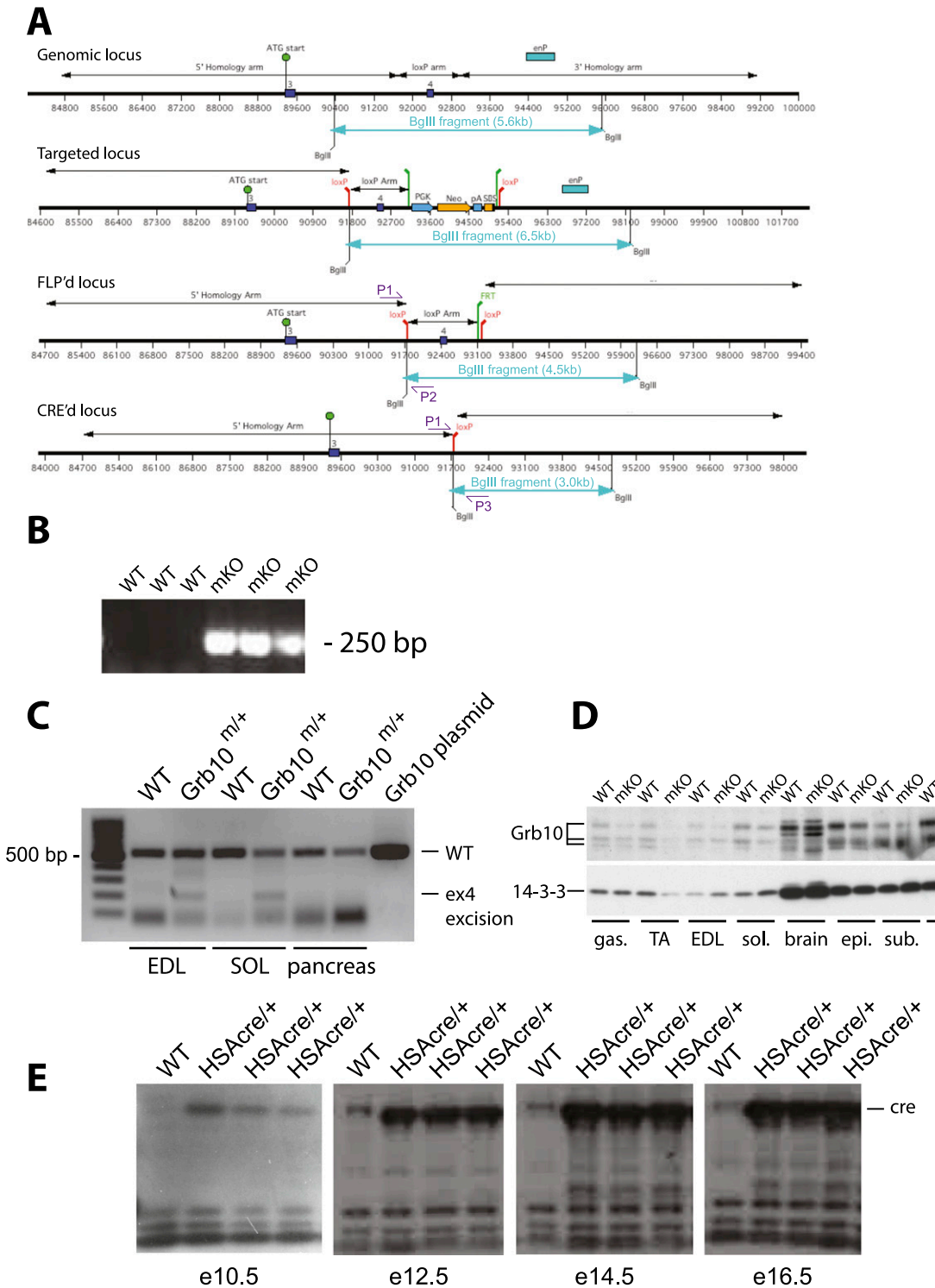

Figure 1. Construction of Grb10-mKO mice by HSA-Cre–mediated excision of exon 4. (A) Schematic diagram of the Grb10 locus targeted, showing location of start site in exon 3 and region bounding exon 4 for excision, as well as primer sites (P1, P2, P3) for PCRs. (B) Agarose gel of PCR from genomic DNA from TA muscle to confirm exon 4 excision. A band of 250 bp indicates excision has occurred. (C) Agarose gel of real-time PCR from EDL, soleus, and pancreas to confirm deletion of exon 4 from mRNA samples of muscle. (D) Western blot analysis of muscle (gastrocnemius, TA, EDL, soleus), brain, and fat (epididymal, subcutaneous, retroperitoneal) to confirm ablation of Grb10 protein in muscle only. (E) Western blot analysis of embryonic tissue (e10.5 to e16.5) to detect cre expression.

Analytical methods

Blood and plasma glucose levels were determined with an Accu-Chek II glucometer (Roche Diagnostics, Castle Hill, Australia). Insulin levels were determined with a mouse insulin enzyme-linked immunosorbent assay (CrystalChem, Downers Grove, IL). Nonesterified fatty acids (NEFAs) were measured with a NEFA-C kit (Wako Pure Chemical Industries, Chuo-ku, Osaka, Japan). Lactate in plasma was determined after protein

precipitation with 6% perchloric acid and neutralizing with 1 M NaOH by measuring production of reduced nicotinamide adenine dinucleotide from oxidized nicotinamide adenine dinucleotide by lactate dehydrogenase in the presence of 0.4 M hydrazine hydrate. Muscle triglyceride and glycogen content were measured as described previously (17, 18). The rate of basal and clamp glucose disappearance (R_d) was determined with steady-state equations. Clamp hepatic glucose output was determined by subtracting the glucose infusion rate from R_d. Glucose uptake into tissues was determined via the following equation:

$$Rg\prime = \left(2\left[^{14}C\right]DGP_{tissue} \Big/ AUC\,2\left[^{14}C\right]DG_{plasma}\right) * [\text{arterial glucose}]$$

where $2[^{14}C]DGP_{tissue}$ is the $2[^{14}C]$DGP radioactivity in the muscle (in dpm/g), AUC $2[^{14}C]DG_{plasma}$ is the area under the plasma $2[^{14}C]$DG disappearance curve (in dpm/min/mL), and [arterial glucose] is the average blood glucose (in mmol/L) (19).

Tissue processing and analysis

For DNA extraction, ear-clip samples were processed with a Qiaxtractor instrument (Qiagen) and Qiagen DX reagents. Genotyping was carried out by real-time polymerase chain reaction (PCR) with several primer pairs. To determine the presence of the floxed allele, the primer pair was 5′ CTAATAAAGAAGGAGGATTCTGTG 3′ (P1, within the 5′ homology arm) and 5′ GTTGTGATACGTGAGGAAGTCGTTCC 3′ (P2, within the loxP arm) (Fig. 1A). To determine excision of exon 4, the primer pair was 5′ CTAATAAAGAAGGAGGATTCTGTG 3′ (P1) and 5′ GCATTCCTCAGTCTGGTGAGAGGC 3′ (P3, within the 3′ homology arm). Presence of HSA-Cre was determined with the combination of primers 5′ CCGGTCGATGCAACGAGTGAT 3′ and 5′ ACCAGAGTCATCCTTAGCGCC 3′. For RNA and protein collection, animals were euthanized by carbon dioxide asphyxiation, and then tissues were collected and immediately snap frozen in liquid nitrogen. RNA extractions from tissue were carried out with the standard Trizol technique. Complementary DNA (cDNA) was synthesized from 2 μg of DNase-treated RNA with Qiagen's Omniscript reverse transcription kit and random 9mers (New England Biolabs, Ipswich, MA). cDNA was amplified by conventional PCR with Phusion-HF polymerase (New England Biolabs) under the following conditions: 98°C 30 seconds, 98°C 10 seconds, 64°C 30 seconds, 72°C 30 seconds for 35 cycles, and 72°C 5 minutes. The PCR products were run on a 2% agarose gel and visualized with Gel Red (Biotium, Freemont, CA). To amplify cDNA, the primer pair was 5′ CCGTGGAAAGCCTTAACTCA 3′ (within exon 3) and 5′ CATCTTCACTAAAGACTTTGACATCC 3′ (within exon 6). Quantitative PCR analysis was performed on 400 ng of RNA per sample with the Qiagen RT^2 Myogenesis and Myopathy PCR array according to the manufacturer's instructions. The PCR plates were run on the Roche LC480 system, and relative expression was quantified by the ΔΔCT method. Expression was normalized to an average of five housekeeping genes (β-actin, β-microglobulin, GAPDH, β-glucuronidase, and HSP90).

For protein analysis, frozen tissues were solubilized (after powdering in the case of muscle) for 2 hours at 4°C in modified radioimmunoprecipitation assay buffer (65 mM Tris, 150 mM NaCl, 5 mM EDTA, 0.1% Nonidet P-40, 0.5% sodium deoxycholate, 0.1% sodium dodecyl sulfate, 10% glycerol, pH 7.4) supplemented with protease and phosphatase inhibitors (10 μg/μL aprotinin, 10 μg/μL leupeptin, 20 mM NaF, 1 mM Na orthovanadate, 1 mM phenylmethylsulfonyl fluoride). Cleared tissue lysates were resolved by sodium dodecyl sulfate polyacrylamide gel electrophoresis and immunoblotted with antibodies (Table 1) against Grb10 (L.J.H.; AB_2721035), the IR β-subunit (BD Transduction Laboratories; AB_397516), phospho-IR (pY1162/3, Biosource; AB_2533762), insulin receptor substrate (IRS-1) (Upstate; AB_2127890), phospho IRS-1/2 (pY612, Biosource; AB_2533768), Akt (AB_329827), phospho Akt (pT308; AB_329825) (both Cell Signaling Technology, Danvers, MA), and cre (Covance, Princeton, NJ; AB_2565079) or 14-3-3 (pan) (Cell Signaling Technology; AB_10860606). The Grb10 antibody is a rat monoclonal antibody and was created by immunizing rats with GST-Grb10 fusion protein (full-length mouse Grb10) by the Monash Antibody Technologies Service, Melbourne. Positive hybridoma clones were screened against the Grb10-SH2 domain, and only negative-interacting clones were selected for further expansion. The antibody is available upon request from L.J.H. Quantitation of immunolabeled bands was performed with IP Laboratory Gel H (BD Biosciences).

Table 1. Antibody Table

Peptide/Protein Target	Name of Antibody	Manufacturer, Catalog No., and/or Name of Individual Providing the Antibody	Species Raised in; Monoclonal or Polyclonal	Dilution Used
Grb10	Anti-Grb10 (full-length mouse Grb10)	L.J. Holt	Rat; polyclonal	1:500
IR	Mouse anti–insulin receptor beta antibody	BD Biosciences, 610110	Mouse; monoclonal	1:2000
Phospho-IR	Phospho-IR/IGF1R (Tyr1162, Tyr1163)	Invitrogen, Thermo Fisher, 44-804G	Rabbit; polyclonal	1:1000
IRS-1	Anti-IRS1 antibody	Upstate, Merck, 06-248	Rabbit; polyclonal	1:1000
Phospho-IRS1/2	Anti-IRS1 (pY612) antibody	Invitrogen, Thermo Fisher, 44-816G	Rabbit; polyclonal	1:1000
Akt	Akt antibody	Cell Signaling Technology, 9272	Rabbit; polyclonal	1:1000
Phospho-Akt	Phospho-Akt (Ser473)	Cell Signaling Technology, 9271	Rabbit; polyclonal	1:1000
Cre	Purified anti-Cre recombinase antibody	Covance, PRB-106P	Rabbit; polyclonal	1:1000
Fourteen-three-three	14-3-3 (pan)	Cell Signaling Technology, 8312	Rabbit; polyclonal	1:1000
α-laminin	Laminin α-2	Santa Cruz, sc-59854	Rat; monoclonal	1:200

Histology and immunofluorescence

Whole 10-mm transverse cryosections of the tibialis anterior (TA) muscle were immunostained with α2 laminin antibody (AB_784266) to localize the fiber boundary. Fluorescent images were captured with a Carl Zeiss AxioImager.Z2 microscope, monochrome CoolCube 1m camera (MetaSystems, Altlussheim, Germany), and Metafer4FL scanning software (MetaSystems). Images (objective 20×) were stitched together in VSlide (MetaSystems), and stitched whole muscle fluorescent images were captured with VSViewer (MetaSystems). Myofiber cross-sectional area was analyzed and calculated as described (20) with MetaMorph software (Molecular Devices).

Statistical analysis

Data are expressed as means ± standard error of the mean (SEM). Differences between groups were determined by *t* test or two-way analysis of variance (ANOVA) as needed. If the two-way ANOVA reached significance, a Sidak *post hoc* test was conducted.

All statistical analysis was done with GraphPad Prism (Version 6 for Windows; GraphPad Software, San Diego, CA). Significance was set at $P \leq 0.05$.

Results

Production of mice with ablation of Grb10 specifically in muscle (Grb10-mKO)

To characterize the autonomous role of Grb10 in muscle, we crossed female Grb10$^{flox/flox}$ mice with male mice expressing Cre recombinase under the control of the HSA promoter to excise exon 4 of Grb10 in muscle (Fig. 1A). The HSA gene is specifically expressed in striated muscles, heart, and skeletal muscle (21, 22).

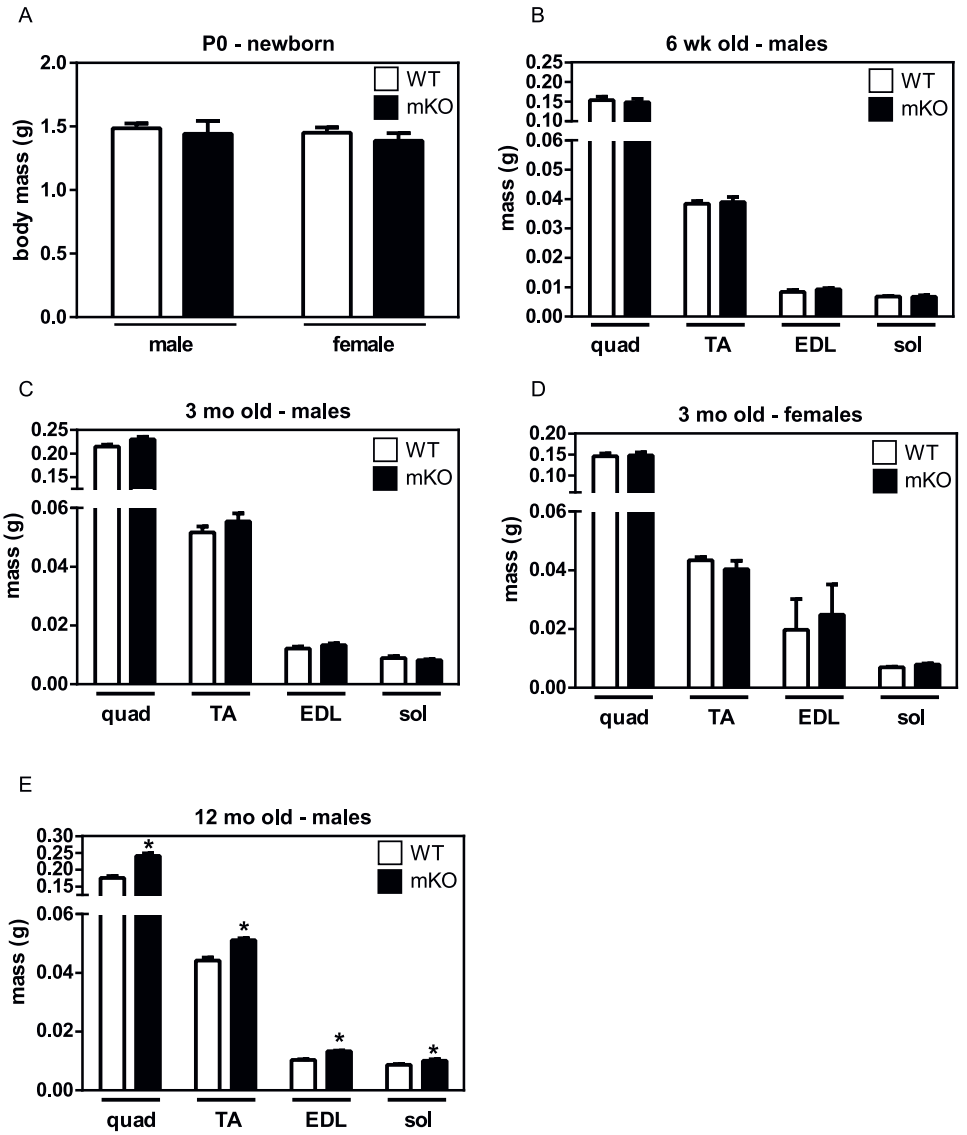

Figure 2. Hypermuscularity becomes apparent in Grb10-mKO mice late in life. (A) Whole body weight for newborn mice on the day of birth (P0). Muscles were dissected from WT and Grb10-mKO mice of various ages and wet weights determined. Muscle weights are shown for (B) male mice aged 6 weeks (WT n = 5, mKO n = 4), (C) male mice aged 3 months (WT n = 10, mKO n = 14), (D) female mice aged 3 months (WT n = 14, mKO n = 19), and (E) male mice aged 12 months (WT n = 12, mKO n = 11). Values are expressed as means ± SEM. *$P < 0.05$ vs WT (*t* test).

Excision was confirmed in genomic DNA from TA muscle, as indicated by a 250-bp band (Fig. 1B) arising from PCR with primers P1 and P3 (Fig. 1A). Real-time PCR analysis also confirmed that Grb10 was disrupted by excision in both white [extensor digitorum longus (EDL)] and red (soleus) muscles but not other tissues, such as pancreas (Fig. 1C). Furthermore, we confirmed that the Grb10 protein was depleted in muscle, including gastrocnemius, TA, EDL, and soleus but not in other tissues such as brain or adipose tissue (Fig. 1D) or liver, kidney, or heart (not shown). Cre recombinase expression was apparent in embryonic tissue at e10.5 to e16.5 (Fig. 1E).

Hypermuscularity with age in Grb10-mKO mice

We have previously shown that germline deletion of Grb10 causes hypermuscularity as determined by limb cross-sectional area in KO mice throughout life (newborn, 3, 6, and 12 months of age) (6). Therefore we examined the size of muscles of Grb10-mKO mice at specific ages (Fig. 2). The total body weight of newborn pups was similar between WT and Grb10-mKO (Fig. 2A). There was also no difference between genotypes in the size of muscles at 6 weeks of age (Fig. 2B, male mice). When mice had matured at 3 months of age, there was again no significant size difference between WT and Grb10-mKO for either male or female mice in any of the four muscle types examined (quadriceps, TA, EDL, and soleus Fig. 2C, 2D). However, at 12 months of age, mice with a muscle-specific Grb10 ablation did exhibit a significant increase in muscle mass, compared with WT, for all four muscle types examined (Fig. 2E). The percentage increases were quad 137%, TA 116%, EDL 128%, and soleus 114%. To determine the underlying cause, TA muscles were further analyzed by examination of fiber size and number. Consistent with the similarity in overall TA muscle mass for 3-month-old mice, there was no significant difference in fiber size or number between genotypes (Fig. 3A, 3C, 3D). However, 12-month-old mice had a significant increase in fiber size in the TA muscle of Grb10-mKO mice compared with WT mice (Fig. 3B, 3C). The number of fibers was similar between genotypes in this age group (Fig. 3B, 3D), and there was no significant difference in fiber type composition between genotypes (data not shown).

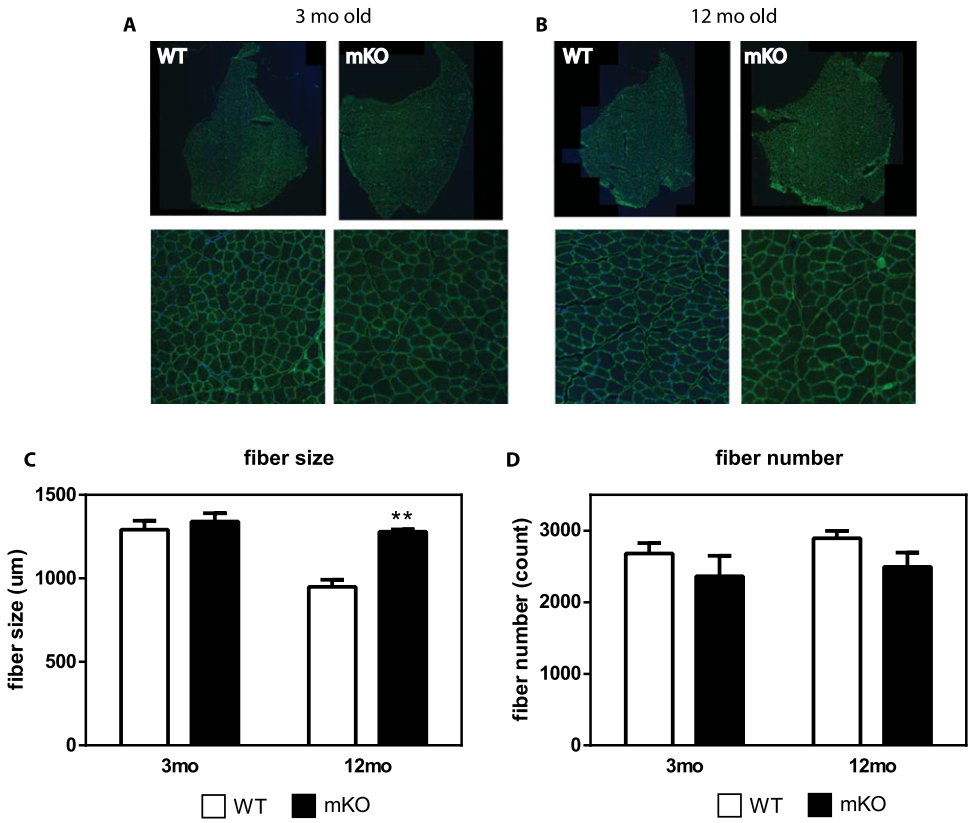

Figure 3. Hypermuscularity of Grb10-mKO mice is caused by enlarged myofiber size. TA muscles dissected from 3-month-old and 12-month-old male mice were sectioned through the midbelly region. (A and B) Representative images of α-laminin stained sections to compare WT and Grb10-mKO total muscle cross-sectional area at ×2.5 and fiber morphology at ×20 magnification. (C) Fiber size and (D) fiber number for TA muscles from WT and Grb10-mKO. Values are expressed as means ± SEM; n = 2 WT, n = 3 mKO for 3-month-old mice; n = 4 WT, n = 3 mKO for 12-month-old mice. $^{**}P < 0.01$ vs WT (ANOVA).

Because 12-month-old mice displayed an altered muscle phenotype upon Grb10 deletion, this age group was used for additional studies with respect to insulin action, to assess the autonomous role of Grb10 in muscle in relation to insulin signaling.

Whole body glucose homeostasis

Previously, we have shown that germline deletion of Grb10 produces mice that have improved glucose tolerance compared with WT mice because of a combination of increased muscle mass and insulin signaling in muscle (3). To determine whether ablation of Grb10 in muscle alone could affect whole body glucose homeostasis, we performed glucose tolerance tests. We found that male mice 3 months old responded similarly to glucose whether they had Grb10-depleted muscle (Fig. 4A, 4B). There was also no difference in glucose tolerance in WT and Grb10-mKO female mice at the same age (data not shown). Because 12-month-old Grb10-mKO mice had bigger muscles, glucose homeostasis was also assessed in mice at this age. At 12 months of age WT and Grb10-mKO mice responded similarly to a glucose load (Fig. 4C, 4D). Although there was no difference in glucose tolerance at the whole body level, this does not preclude effects at the level of the muscle itself. Therefore, a more detailed assessment of insulin action in Grb10-mKO mice at 12 months of age was carried out.

Assessment of insulin action

In the first instance glucose metabolism under basal conditions was determined. There was no difference in whole body glucose disappearance between the two genotypes (Fig. 5A). Nor was there any difference in glucose uptake into discrete tissues, such as quadriceps muscle, gastrocnemius muscle, epididymal fat, subcutaneous fat, or heart under these conditions (Fig. 5B). The plasma levels of both glucose and insulin were comparable for WT and Grb10-mKO animals in the basal state (glucose: WT 8.0 ± 0.4 mM, Grb10-mKO 8.2 ± 0.5 mM; insulin: WT 30.5 ± 9.1 μU/μL, Grb10-mKO 39.2 ± 5.7 μU/μL).

To determine whether disruption of Grb10 in muscle affects insulin action when insulin is increased, hyperinsulinemic-euglycemic clamp studies were performed. Plasma measurements confirmed that insulin levels were similarly elevated, and fatty acid levels similarly suppressed for both WT and Grb10-mKO cohorts during the clamp (Table 2), and that whole body glucose disposal was elevated compared with basal with the infusion of exogenous insulin (Fig. 5C). The glucose infusion rate, a measure of whole body insulin sensitivity, was significantly higher in Grb10-mKO animals compared with WT mice (Fig. 5D). In addition, glucose uptake into quadriceps and gastrocnemius muscles was significantly elevated in the Grb10-mKO mice (Fig. 5E).

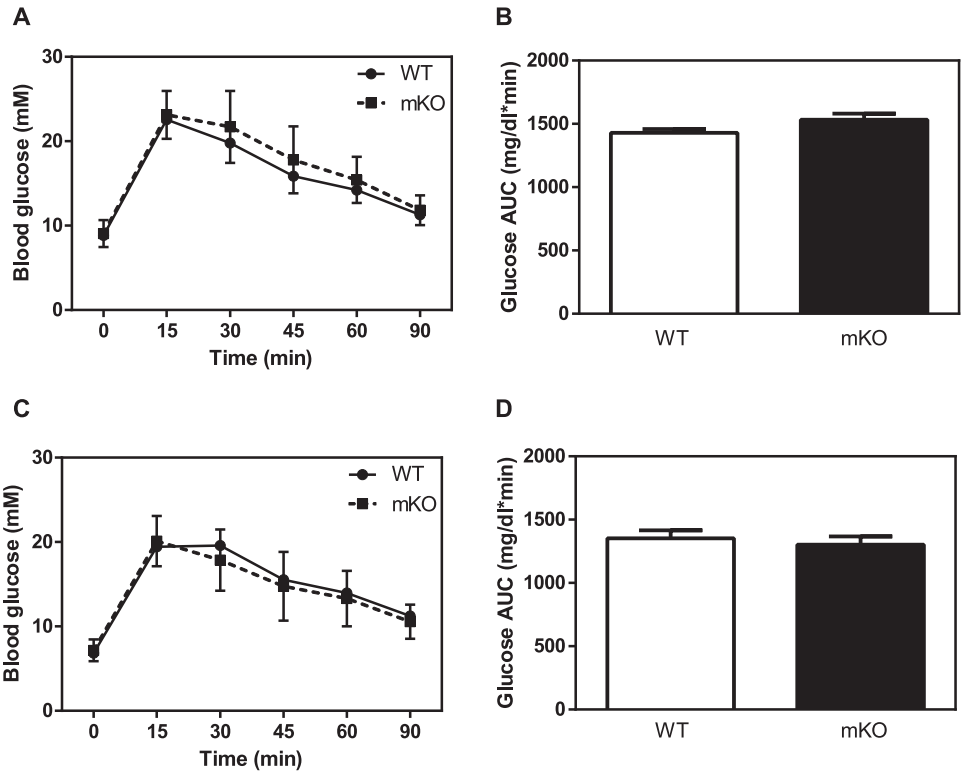

Figure 4. Whole body glucose homeostasis of Grb10-mKO mice. Glucose tolerance tests were performed for (A) 3-month-old mice and (C) 12-month-old mice. (B and D) Quantification of the total area under the curve for total glycemic excursions for the same groups of mice, respectively. Values are expressed as means ± SEM; n = 19 for WT, n = 22 for mKO (3 months old); n = 15 for WT, n = 14 for mKO (12 months old). No significant difference vs WT for either age group.

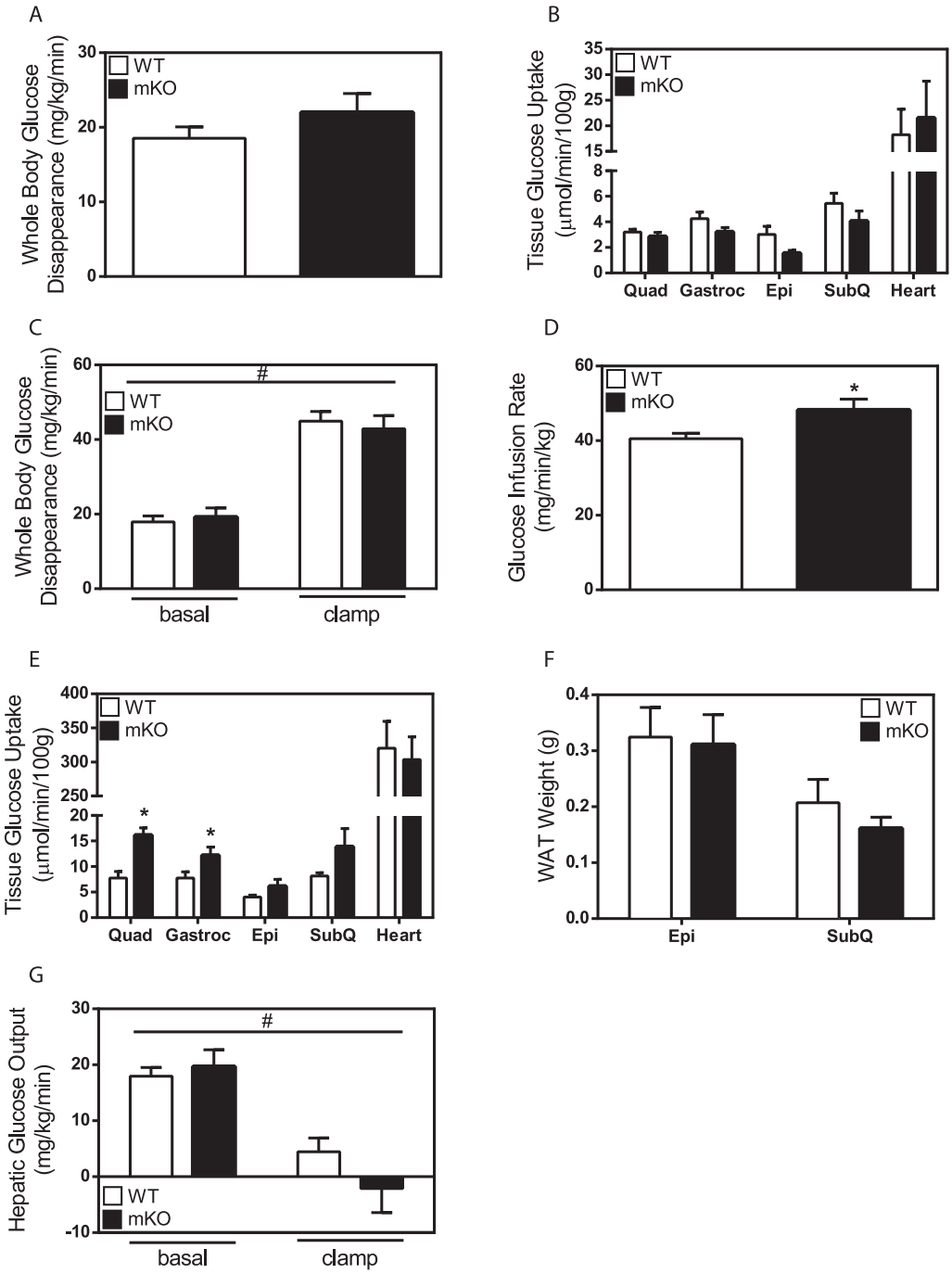

Figure 5. Grb10-mKO mice have increased insulin sensitivity. Basal measurements for (A) whole body glucose disappearance and (B) tissue glucose uptake. Measurements determined under hyperinsulinemic-euglycemic clamp conditions for (C) insulin-stimulated whole body glucose disappearance, (D) glucose infusion rate, (E) tissue glucose uptake, and (G) hepatic glucose output. (F) Weight of adipose tissue depots (WAT) from WT and Grb10-mKO mice. Animals were 12 months old. Values are expressed as means ± SEM; n = 6 for WT, n = 6 for mKO. Direct comparison between WT and Grb10-mKO was performed with a *t* test, $^{*}P < 0.05$. When the effects of insulin and genotype were examined, a two-way ANOVA was used to test for significant differences. Different from basal period, $^{\#}P < 0.05$ (two-way ANOVA). Epi, epididymal fat; Gastroc, gastrocnemius; Quad, quadriceps; SubQ, subcutaneous fat.

Plasma lactate levels were not different between WT and Grb10-mKO animals in the basal state (Table 2). However, plasma lactate was significantly elevated in clamped animals. Grb10-mKO animals displayed significantly higher plasma lactate compared with WT at the end of the hyperinsulinemic-euglycemic clamp procedure (Table 2). There was no difference in the size of epididymal or subcutaneous adipose depots from WT and Grb10-mKO mice (Fig. 5F) and no difference in glucose uptake in these adipose tissue depots (Fig. 5E). There was no difference in glucose uptake in the heart of WT and Grb10-mKO mice (Fig. 5E). The liver was also unaffected

Table 2. Fasting and Insulin Clamp Characteristics of WT and Grb10-mKO Mice

	WT	Grb10-mKO
Blood glucose, mM		
Basal	7.0 ± 0.3	7.3 ± 0.4
Clamp	7.5 ± 0.2	8.1 ± 0.3
Plasma insulin, μU/mL		
Basal	23.6 ± 4.4	20.5 ± 5.3
Clamp	65.0 ± 5.0	70.0 ± 9.0[a]
NEFA, mM		
Basal	0.73 ± 0.03	0.63 ± 0.05
Clamp	0.21 ± 0.02	0.20 ± 0.04[a]
Plasma lactate, mM		
Basal	0.63 ± 0.12	0.47 ± 0.09
Clamp	1.07 ± 0.08	1.82 ± 0.05[a,b]

Data presented as mean ± SEM; n = 5 for WT, n = 6 for mKO.

[a]Effect of clamp conditions, $P < 0.01$ (two-way ANOVA).

[b]Effect of genotype, $P < 0.01$ (two-way ANOVA).

by Grb10 deletion in muscle because hepatic glucose output in the basal and insulin-stimulated state was comparable between WT and Grb10-mKO animals (Fig. 5G). Although there was increased glucose uptake into muscle, there was no difference between genotypes in total glycogen content or triglyceride content in muscle at 12 months of age (Fig. 6A, 6B).

Grb10 ablation in muscle leads to altered insulin signaling without changes in the expression of key genes involved in glucose metabolism

Because insulin action in muscle was increased in Grb10-mKO mice during the hyperinsulinemic-euglycemic clamp, we examined signaling events in muscle that could be responsible for this change (Fig. 7A). A significant reduction in muscle Grb10 expression was confirmed by Western blot (Fig. 7A, 7B). There was no significant difference between WT and Grb10-mKO animals for the phosphorylation status of the IR in the basal state or at the end of the hyperinsulinemic clamp (Fig. 7C). IRS-1 phosphorylation was higher in Grb10-mKO muscle in the basal and insulin-stimulated states (Fig. 7D), and Akt phosphorylation was also higher for Grb10-depleted muscle before and after 2 hours of stimulation at the physiological level of insulin used for the clamp studies (Fig. 7E).

Gene expression analysis with a myogenesis and myopathy panel showed no difference in fiber type gene signatures for fast-twitch (*atp2a1, myh2, tnni2, tnnt3*) and slow-twitch (*mb, myh1, tnnc1, tnnt1*) fibers between Grb10-mKO and WT quadriceps muscle (Fig. 8). Similarly, there was no change in the expression of genes involved in glucose uptake (*slc2a4*), phosphorylation (*hk2*), and oxidation (*pdk4, cs*). However, inhibitors of myogenesis (*mstn, nfkb1*) were downregulated in the muscle of Grb10-mKO mice.

Discussion

Grb10 is an adaptor protein that associates with a variety of receptor tyrosine kinases, and therefore Grb10 has considerable potential to influence multiple signaling pathways in many tissues. Previous studies using global KO mouse models have determined that deletion of Grb10 leads to a significant increase in body size and in particular increased muscle mass, which contributes to increased glucose tolerance and insulin sensitivity (3, 4, 7). Grb10 is not expressed ubiquitously and is more abundant in muscle, adipose tissue, pancreas, and brain (3, 4). Also, the gene encoding Grb10 protein is an imprinted gene with the maternal allele producing messenger RNA (mRNA) for translation in most tissues except the brain, where Grb10 protein is expressed from the paternal allele (3). The imprinting of Grb10 gene expression and the macrosomia present during embryogenesis and neonatal development suggest that multiple effects of Grb10 deletion could lead to the presence of the larger muscle mass and increased muscle fiber number observed in the global deletion model. The current results provide significant information on the effects of deletion of Grb10 specifically in muscle and also raise some interesting questions about the timing of Cre recombinase activity in the production of gene deletion in muscle.

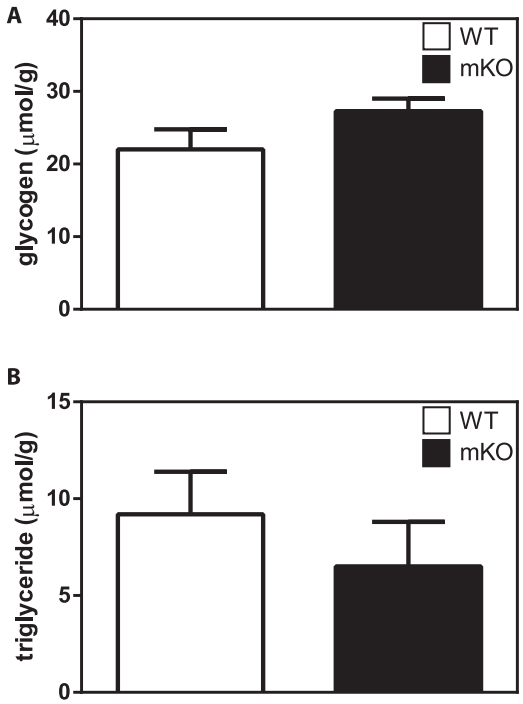

Figure 6. Grb10-mKO mice do not have significantly altered metabolic storage properties of muscle. (A) Glycogen content and (B) triglyceride content of muscle in 12-month-old mice. Values are expressed as means ± SEM; n = 5 for WT, n = 5 for mKO. No significant difference vs WT by *t* test.

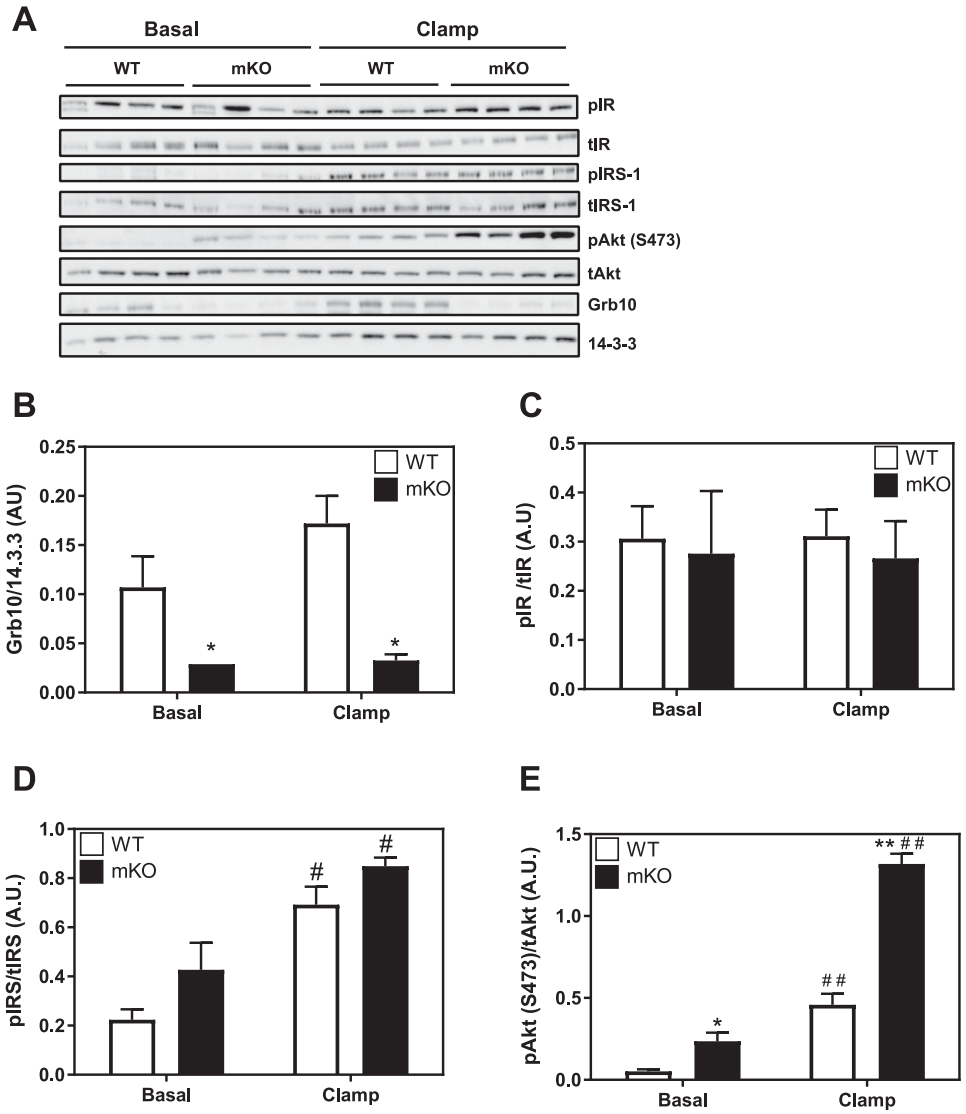

Figure 7. Insulin-induced signaling in Grb10-mKO animals. Muscles collected after the hyperinsulinemic-euglycemic clamp were analyzed by Western blotting to determine the phosphorylation status of major components of the insulin signaling pathway. After densitometric analysis, protein phosphorylation was normalized with protein loading. Values are expressed as means ± SEM; n = 4 for WT, n = 4 for mKO. Effect of clamp, $^{\#}P < 0.01$; $^{\#\#}P < 0.0001$. Effect of genotype, $^{*}P < 0.01$; $^{**}P < 0.0001$ (two-way ANOVA).

In the current work HSA-Cre was used to produce deletion of Grb10 specifically in muscle fibers. The presence of Cre was detected at day 10.5 of embryogenesis, and mice used in these studies clearly have a muscle-specific deletion of Grb10. Various other muscle-specific transgenic Cre mice have been used to produce muscle-specific deletion of genes. These include Cre recombinase expression under the control of the promoters for muscle creatine kinase, myogenic factor 5, myogenin, myosin light chain 1/3 fast, and paired box gene 7 (23). All these have been measured as expressing Cre recombinase in embryos at 9 to 10 days postcoitum, with one report describing detection of skeletal actin expression in muscle somites as early as 8 days postcoitum (24). It therefore appears that the deletion of Grb10 in the current model is occurring at a very early stage of striated muscle development in the embryo. Although not definitive, the results reported here probably represent the effects of muscle lineage–specific deletion of Grb10 from the earliest possible point in development.

The overall phenotype of the Grb10-mKO mice was significantly different from that of the global Grb10-KO previously reported by us and others (3, 4, 6, 7). Grb10-mKO mice were the same size at birth as WT littermates, and there was no detectable difference in body weight, tissue weights (including muscle), or metabolic measures such as glucose tolerance ≤3 months of age. However, in animals euthanized at 12 months of age there was a consistent increase in muscle size that was the result of an increase in muscle fiber cross-sectional area. This was different from the increased muscle size seen from early in the life of Grb10 global KO mice, which was caused by more muscle fibers (6). These differences indicate that

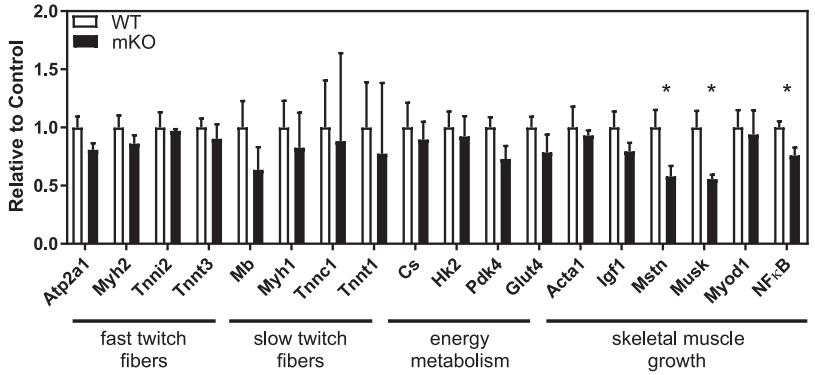

Figure 8. Gene expression in Grb10-mKO muscle. Gene expression analysis was performed on quadriceps muscle from 12-month-old mice after a 5-hour fast in the basal state. Selected genes were chosen from the Qiagen RT^2 Myogenesis and Myopathy PCR array and analyzed by the ΔΔCT method. Expression was normalized to an average of five housekeeping genes (β-actin, β-microglobulin, GAPDH, β-glucuronidase, and HSP90). Values are fold change compared with WT, means ± SEM, n = 5. Analyzed by individual *t* tests. $^*P < 0.05$.

the larger-muscle phenotype observed in the Grb10 global KO did not result specifically from the deletion of Grb10 in muscle but must also be related to Grb10 deletion at earlier time points in muscle or in other tissues and perhaps the general macrosomia observed in the global Grb10 KO mice. Consistent with the Grb10 global KO mice (6), there were no differences in the distribution of fiber types between muscle from Grb10-mKO and WT mice, analyzed by gene expression (Fig. 8) or histology (not shown).

There are several other models of tissue-specific deletion of Grb10. In mice with a global deletion of Grb10, muscle mass was higher but adipose mass was lower compared with WT mice. However, deletion of Grb10 specifically in adipose tissue leads to larger adipose tissue mass when mice were fed a high-fat diet, reportedly via suppression of lipolysis and changes in energy expenditure, but there were no reported differences in the size of other organs or tissues (12). Deletion of Grb10 specifically in the pancreas led to an increase in pancreas size and increased beta cell mass without observed changes in other tissues. These changes in the pancreas protected against streptozotocin-induced beta cell apoptosis and suggested a critical role for Grb10 in regulating beta cell growth and function (11). These studies suggest that the specific role of Grb10 in individual tissues can be different from the combined effect of global deletion of this signaling adaptor protein.

In studies involving global deletion of the Grb10 gene, the hypermuscular phenotype was associated with an increase in muscle fiber number and an increase in body size (nasoanal length) (6). The extent of the hypermuscularity observed in the muscle-specific Grb10-mKO mice described here was less than the global KO, was not evident until the mice were 6 to 12 months of age, and was characterized by an increase in muscle fiber size rather than fiber number, as in global Grb10 KO mice (6). Although the hypermuscular phenotype of the Grb10-mKO is not entirely consistent with that described for global deletion of Grb10, it is consistent with the role of Grb10 as an adaptor protein regulating signaling via tyrosine kinase receptors such as the insulin and IGF-1 receptors. In previous reports increased phosphorylation of Akt was observed in muscle of mice with global deletion of Grb10 when they were stimulated with supraphysiological doses of insulin or at the end of a hyperinsulinemic-euglycemic clamp (4). In the current study increased phosphorylation of Akt was also present in the basal and insulin-stimulated state in muscle of Grb10-mKO mice, and this phosphorylation was accompanied by an increase in insulin-stimulated glucose uptake in muscle during a hyperinsulinemic-euglycemic clamp and a small but significant increase in whole body glucose infusion rate under clamp conditions. Similarly, plasma lactate (which usually rises during a clamp because of the higher rate of glucose disposal) (25) was further elevated in Grb10-mKO mice (Table 2). This difference is probably a consequence of the increase in muscle glucose uptake observed in clamped Grb10-mKO animals (Fig. 5E). The increase in mass of specific muscles ranged from 14% to 37%, and therefore the changes in whole body glucose turnover observed in Grb10-mKO mice could result from an increased muscle mass. However, the increase in insulin-stimulated glucose uptake measured in muscle per unit mass was ~70% to 100% in Grb10-mKO mice, and therefore we conclude that changes in whole body glucose disposal are more likely to be the result of an increase in insulin action in muscle *per se* rather than similar insulin action in an increased amount of muscle.

The increase in basal and insulin-stimulated insulin signaling at the level of Akt is likely to be the result of the absence of Grb10 negative modulation of phosphorylation at the level of the insulin receptor, as previously demonstrated (3). Therefore, the higher insulin-stimulated glucose uptake in Grb10-mKO muscle compared with WT may be caused by the corresponding elevation in the phosphorylation of Akt, which would probably lead to an increase in GLUT4 translocation mediated by TBC1D4 (26). Knockdown of Grb10 in muscle did not alter the mRNA expression of GLUT4 (*slc2a4*), hexokinase 2 (*hk2*), or citrate synthase (*cs*) (Fig. 8), and therefore differences in insulin-stimulated glucose uptake between Grb10-mKO and WT muscle are probably mediated by the posttranslational regulation of insulin signaling discussed above rather than

the abundance of enzymes involved in glucose metabolism. The consequences of a chronic increase in growth factor signaling could explain the increase in fiber size and muscle mass seen in the older Grb10-mKO mice. Acute overexpression of a constitutively active construct of Akt via *in vivo* electroporation is sufficient to increase fiber size in rat skeletal muscle (27, 28), and therefore it seems reasonable to conclude that a chronic elevation of Akt phosphorylation would produce greater stimulation of transcriptional pathways regulating muscle fiber size. Interestingly, gene expression of the inhibitors of myogenesis, myostatin and NF-κB, were decreased in the muscle of Grb10-mKO mice, suggesting possible regulation by Grb10 through altered insulin/IGF-1 signaling.

Although Grb10 deletion specifically in muscle does produce a phenotype of increased muscle size, it is clear that this phenotype (which does not become evident until the mice are 6 to 12 months of age) is different from the increased muscle size of global Grb10 KO mice observed during embryogenesis, neonatal development, and adulthood (3, 4, 6). This finding suggests that the global deletion of Grb10 has effects at the earliest stages of development of the embryo that promote a generalized macrosomia and increase muscle fiber number. The deletion of Grb10 only in muscle requires a myocyte-specific Cre recombinase, and therefore the deletion of the Grb10 gene occurs at a time point when muscle cells start to develop, which is a significantly later embryonic stage than the global deletion.

The muscle phenotypes produced by the global deletion and muscle-specific deletion of Grb10 were different, but muscle from both lines displayed an increase in proximal insulin signaling, most obvious at the level of Akt. This molecular phenotype in Grb10-deleted muscle adds to the evidence for Grb10 having a role as a negative modulator of tyrosine kinase receptor signaling and suggests that manipulation of Grb10 function specifically in muscle could affect muscle size and function, particularly as animals age. Our findings suggest that careful consideration should be given to including regulation of Grb10 activity in any strategies aimed at increasing muscle size and insulin action to combat the effects of aging.

Acknowledgments

The authors thank the Biological Testing Facility at the Garvan Institute of Medical Research for assistance with animal care and the Australian Phenomics Network Histopathology and Organ Pathology Service at the University of Melbourne.

Financial Support: L.J.H. and N.M. were supported by NHMRC Grant 1009794. G.J.C. and R.J.D. were supported by research fellowships from the NHMRC. N.T. was supported by an Australian Research Council Future Fellowship. L.S. was supported by an Australian Postgraduate Award. A.E.B, E.S., E.P., and D.W. were supported by NHMRC program Grant 53921. J.D.W. and C.A.C. were supported by Muscular Dystrophy Australia, Murdoch Children's Research Institute, and Victorian Government's Operational Infrastructure Support Program. The contents of the published material are solely the responsibility of the Garvan Institute of Medical Research and do not reflect the views of the NHMRC.

Correspondence: Gregory J. Cooney, PhD, Diabetes and Metabolism Division, Garvan Institute of Medical Research, 384 Victoria Street, Darlinghurst, New South Wales 2010, Australia. E-mail: g.cooney@garvan.org.au; or Roger J. Daly, PhD, Department of Biochemistry and Molecular Biology, Monash Biomedicine Discovery Institute, Monash University, Level 1, Building 77, Clayton Campus, 23 Innovation Walk, Clayton, Victoria 3800, Australia. E-mail: roger.daly@monash.edu.

Disclosure Summary: The authors have nothing to disclose.

References

1. Holt LJ, Siddle K. Grb10 and Grb14: enigmatic regulators of insulin action—and more? *Biochem J*. 2005;**388**(Pt 2):393–406.
2. Depetris RS, Hu J, Gimpelevich I, Holt LJ, Daly RJ, Hubbard SR. Structural basis for inhibition of the insulin receptor by the adaptor protein Grb14. *Mol Cell*. 2005;**20**(2):325–333.
3. Smith FM, Holt LJ, Garfield AS, Charalambous M, Koumanov F, Perry M, Bazzani R, Sheardown SA, Hegarty BD, Lyons RJ, Cooney GJ, Daly RJ, Ward A. Mice with a disruption of the imprinted Grb10 gene exhibit altered body composition, glucose homeostasis, and insulin signaling during postnatal life. *Mol Cell Biol*. 2007;**27**(16):5871–5886.
4. Wang L, Balas B, Christ-Roberts CY, Kim RY, Ramos FJ, Kikani CK, Li C, Deng C, Reyna S, Musi N, Dong LQ, DeFronzo RA, Liu F. Peripheral disruption of the Grb10 gene enhances insulin signaling and sensitivity in vivo. *Mol Cell Biol*. 2007;**27**(18):6497–6505.
5. Charalambous M, Smith FM, Bennett WR, Crew TE, Mackenzie F, Ward A. Disruption of the imprinted Grb10 gene leads to disproportionate overgrowth by an Igf2-independent mechanism. *Proc Natl Acad Sci USA*. 2003;**100**(14):8292–8297.
6. Holt LJ, Turner N, Mokbel N, Trefely S, Kanzleiter T, Kaplan W, Ormandy CJ, Daly RJ, Cooney GJ. Grb10 regulates the development of fiber number in skeletal muscle. *FASEB J*. 2012;**26**(9):3658–3669.
7. Holt LJ, Lyons RJ, Ryan AS, Beale SM, Ward A, Cooney GJ, Daly RJ. Dual ablation of Grb10 and Grb14 in mice reveals their combined role in regulation of insulin signaling and glucose homeostasis. *Mol Endocrinol*. 2009;**23**(9):1406–1414.
8. Coleman ME, DeMayo F, Yin KC, Lee HM, Geske R, Montgomery C, Schwartz RJ. Myogenic vector expression of insulin-like growth factor I stimulates muscle cell differentiation and myofiber hypertrophy in transgenic mice. *J Biol Chem*. 1995;**270**(20):12109–12116.
9. Musarò A, McCullagh K, Paul A, Houghton L, Dobrowolny G, Molinaro M, Barton ER, Sweeney HL, Rosenthal N. Localized Igf-1 transgene expression sustains hypertrophy and regeneration in senescent skeletal muscle. *Nat Genet*. 2001;**27**(2):195–200.
10. McPherron AC, Lawler AM, Lee SJ. Regulation of skeletal muscle mass in mice by a new TGF-beta superfamily member. *Nature*. 1997;**387**(6628):83–90.
11. Zhang J, Zhang N, Liu M, Li X, Zhou L, Huang W, Xu Z, Liu J, Musi N, DeFronzo RA, Cunningham JM, Zhou Z, Lu XY, Liu F. Disruption of growth factor receptor-binding protein 10 in the pancreas enhances β-cell proliferation and protects mice from streptozotocin-induced β-cell apoptosis. *Diabetes*. 2012;**61**(12):3189–3198.
12. Liu M, Bai J, He S, Villarreal R, Hu D, Zhang C, Yang X, Liang H, Slaga TJ, Yu Y, Zhou Z, Blenis J, Scherer PE, Dong LQ, Liu F. Grb10

promotes lipolysis and thermogenesis by phosphorylation-dependent feedback inhibition of mTORC1. *Cell Metab*. 2014;**19**(6):967–980.
13. Miniou P, Tiziano D, Frugier T, Roblot N, Le Meur M, Melki J. Gene targeting restricted to mouse striated muscle lineage. *Nucleic Acids Res*. 1999;**27**(19):e27.
14. Brandon AE, Stuart E, Leslie SJ, Hoehn KL, James DE, Kraegen EW, Turner N, Cooney GJ. Minimal impact of age and housing temperature on the metabolic phenotype of Acc2-/- mice. *J Endocrinol*. 2016;**228**(3):127–134.
15. Ayala JE, Bracy DP, McGuinness OP, Wasserman DH. Considerations in the design of hyperinsulinemic-euglycemic clamps in the conscious mouse. *Diabetes*. 2006;**55**(2):390–397.
16. Charbonneau A, Marette A. Inducible nitric oxide synthase induction underlies lipid-induced hepatic insulin resistance in mice: potential role of tyrosine nitration of insulin signaling proteins. *Diabetes*. 2010;**59**(4):861–871.
17. Bruce CR, Hoy AJ, Turner N, Watt MJ, Allen TL, Carpenter K, Cooney GJ, Febbraio MA, Kraegen EW. Overexpression of carnitine palmitoyltransferase-1 in skeletal muscle is sufficient to enhance fatty acid oxidation and improve high-fat diet-induced insulin resistance. *Diabetes*. 2009;**58**(3):550–558.
18. Hoy AJ, Bruce CR, Cederberg A, Turner N, James DE, Cooney GJ, Kraegen EW. Glucose infusion causes insulin resistance in skeletal muscle of rats without changes in Akt and AS160 phosphorylation. *Am J Physiol Endocrinol Metab*. 2007;**293**(5):E1358–E1364.
19. Ayala JE, Bracy DP, Julien BM, Rottman JN, Fueger PT, Wasserman DH. Chronic treatment with sildenafil improves energy balance and insulin action in high fat-fed conscious mice. *Diabetes*. 2007;**56**(4):1025–1033.
20. Garton F, Seto JT, North KN, Yang N. Validation of an automated computational method for skeletal muscle fibre morphometry analysis. *Neuromuscul Disord*. 2010;**20**(8):540–547.
21. Brennan KJ, Hardeman EC. Quantitative analysis of the human alpha-skeletal actin gene in transgenic mice. *J Biol Chem*. 1993;**268**(1):719–725.
22. Muscat GE, Kedes L. Multiple 5′-flanking regions of the human alpha-skeletal actin gene synergistically modulate muscle-specific expression. *Mol Cell Biol*. 1987;**7**(11):4089–4099.
23. McCarthy JJ, Srikuea R, Kirby TJ, Peterson CA, Esser KA. Inducible Cre transgenic mouse strain for skeletal muscle-specific gene targeting. *Skelet Muscle*. 2012;**2**(1):8.
24. Sassoon DA, Garner I, Buckingham M. Transcripts of alpha-cardiac and alpha-skeletal actins are early markers for myogenesis in the mouse embryo. *Development*. 1988;**104**(1):155–164.
25. Yki-Järvinen H, Bogardus C, Foley JE. Regulation of plasma lactate concentration in resting human subjects. *Metabolism*. 1990;**39**(8):859–864.
26. Sakamoto K, Holman GD. Emerging role for AS160/TBC1D4 and TBC1D1 in the regulation of GLUT4 traffic. *Am J Physiol Endocrinol Metab*. 2008;**295**(1):E29–E37.
27. Bodine SC, Stitt TN, Gonzalez M, Kline WO, Stover GL, Bauerlein R, Zlotchenko E, Scrimgeour A, Lawrence JC, Glass DJ, Yancopoulos GD. Akt/mTOR pathway is a crucial regulator of skeletal muscle hypertrophy and can prevent muscle atrophy in vivo. *Nat Cell Biol*. 2001;**3**(11):1014–1019.
28. Cleasby ME, Reinten TA, Cooney GJ, James DE, Kraegen EW. Functional studies of Akt isoform specificity in skeletal muscle in vivo; maintained insulin sensitivity despite reduced insulin receptor substrate-1 expression. *Mol Endocrinol*. 2007;**21**(1):215–228.